Available online at www.sciencedirect.com
SCIENCE DIRECT®
ELSEVIER
International Journal of Multiphase Flow 30 (2004) 419–428
International Journal of Multiphase Flow
www.elsevier.com/locate/ijmulflow

Brief communication

Hydrodynamics of particle segregation in fluidized beds

Dinesh Gera [a,*], Madhava Syamlal [a], Thomas J. O'Brien [b,1]

[a] *Fluent Incorporated, 3647 Collins Ferry Road, Suite A, Morgantown, WV 26505, USA*
[b] *US Department of Energy, 3610 Collins Ferry Road, MS-N04, Morgantown, WV 26505, USA*

Received 14 July 2003; received in revised form 14 November 2003

1. Introduction

Research in multiple particulate phase hydrodynamics is important in many industrial applications that involve segregation or mixing processes, specifically in mineral classification, elutriation, sedimentation, crystallization and fluid bed leaching, just to name a few. There have been several investigations dealing with segregation and mixing of particles of different sizes and densities in fluidized bed reactors or classifiers (Chen et al., 2002). The studies show that particles will segregate into layers if a bed, consisting of two different size particles with the same density, is fluidized with a velocity that is in between the individual minimum fluidization (u_{mf}) velocities for each particle type. The binary system will not segregate if the fluidizing velocity is higher than the u_{mf} of the larger particles; rather the particles mix vigorously. The models reported in the literature are able to predict the segregation of the particles at an intermediate fluidization velocity (Goldschmidt et al., 2001). However, they predict particle segregation even at a low fluidization velocity, when segregation is not observed. In this study we modified the particle–particle drag term so that the model predicts no segregation at low velocities, segregation at intermediate velocities, and mixing at high velocities. Furthermore we show that the predicted rate of segregation at intermediate velocities agrees quantitatively with experimental data.

In the last decade, considerable efforts have been made in developing detailed hydrodynamic tools for the simulation of fluidized bed dynamics, including Eulerian/Lagrangian, and the hybrid Eulerian/Lagrangian mapping methods. Eulerian/Eulerian methods consider the primary and secondary (dispersed) phases to be interpenetrating continua, and the equations employed are generalizations of the Navier–Stokes equations (e.g., Gidaspow, 1994). Eulerian/Lagrangian models describe the primary phase flow using the continuum equations, and the particulate phase

* Corresponding author. Tel.: +1-304-598-7934; fax: +1-304-598-7185.
E-mail addresses: dfg@fluent.com (D. Gera), tobrie@netl.doe.gov (T.J. O'Brien).
[1] Tel.: +1-304-285-4571.

0301-9322/$ - see front matter
doi:10.1016/j.ijmultiphaseflow.2004.01.003

flow is described by tracking the motion of individual particles (e.g., Tsuji et al., 1993; Gera et al., 1998). Lagrangian models include the effects of particle collisions and the forces acting on the particles by the gas.

The focus of this paper is on Eulerian/Eulerian methods for the computation of gas–solids flows. Eulerian/Eulerian methods are potentially faster than Eulerian/Lagrangian methods, but require the formulation of constitutive equations. We extended a two-fluid model (gas and one granular phase) to a multi-fluid model (gas and several granular phases) by adding constitutive equations for the particle–particle drag and the maximum particle packing. The new constitutive equations are added in the MFIX code, an open-source multiphase flow model (Syamlal et al., 1993, www.mfix.org). The model is used to describe solids segregation in a dense fluidized bed.

2. Hydrodynamic model

The mathematical model is based on the assumption that the phases can be mathematically described as interpenetrating continua; the point variables are averaged over a region that is large compared with the particle spacing but much smaller than the flow domain (e.g., Anderson and Jackson, 1967). The equations solved by the MFIX code used in this study are given in Syamlal et al. (1993). The continuity equation for each phase is written as:

$$\frac{\partial}{\partial t}(\varepsilon_m \rho_m) + \nabla \cdot (\varepsilon_m \rho_m \vec{v}_m) = 0 \tag{1}$$

where ρ_m and $\vec{v}_m$ are the density and velocity of the mth phase ($m = 0$ represents the gas phase), respectively, ε_m is the volume fraction of the mth phase with the condition $\sum_m \varepsilon_m = 1$.

The momentum equation for the gas phase is expressed as:

$$\frac{\partial}{\partial t}(\varepsilon_0 \rho_0 \vec{v}_0) + \nabla \cdot (\varepsilon_0 \rho_0 \vec{v}_0 \vec{v}_0) = \nabla \cdot \bar{\bar{S}}_0 + \varepsilon_0 \rho_0 \vec{g} - \sum_{m=1}^{M} \vec{I}_{0m} \tag{2}$$

where the stress tensor for the gas phase is defined as:

$$\bar{\bar{S}}_0 = -P_0 \bar{\bar{I}} + \varepsilon_0 \mu_0 [\nabla \vec{v}_0 + (\nabla \vec{v}_0)^{\mathrm{T}}] + \varepsilon_0 \left(\lambda_0 - \frac{2}{3} \mu_0 \right) \nabla \cdot \vec{v}_0 \bar{\bar{I}} \tag{3}$$

Here P_0 is the gas pressure, μ_0 and λ_0 are the shear and bulk viscosity of the gas phase, $\bar{\bar{I}}$ is a unit tensor, $\vec{I}_{0m}$ is an interaction (or drag) force representing the momentum transfer between the gas phase and the mth solid phase. The interaction force $\vec{I}_{0m}$ is written as:

$$\vec{I}_{0m} = \varepsilon_m \nabla P_0 - F_{0m}(\vec{v}_m - \vec{v}_0) \tag{4}$$

where the interaction–exchange coefficient (F_{0m}) between the gas phase and the mth solid phase is written as (Gidaspow, 1994):

$$F_{0m} = \begin{cases} 150 \frac{\varepsilon_m (1-\varepsilon_0)}{\varepsilon_0 d_{\mathrm{pm}}^2} \mu_0 + 1.75 \varepsilon_m \frac{\rho_0}{d_p} |v_m - v_0| & \text{for } \varepsilon \leqslant 0.8 \\ \frac{0.75 \varepsilon_m \varepsilon_0 \rho_0}{d_{\mathrm{pm}}} C_D |\vec{v}_m - \vec{v}_0| \varepsilon_0^{-2.65} & \text{for } \varepsilon > 0.8 \end{cases} \tag{5}$$

and

$$C_D = \begin{cases} 24(1 + 0.15 Re_m^{0.687})/Re_m, & Re_m < 1000 \\ 0.43, & Re_m \geqslant 1000 \end{cases} \tag{6}$$

where d_{pm} is the particle diameter of the mth solids phase. The Reynolds number for the mth solids phase is given by

$$Re_m = d_{pm}|\vec{v}_m - \vec{v}_0|\rho_0/\mu_0$$

The momentum equation for each of the 'm' solid phases is expressed as:

$$\frac{\partial}{\partial t}(\varepsilon_m\ \rho_m\ \vec{v}_m) + \nabla \cdot (\varepsilon_m\ \rho_m\ \vec{v}_m\ \vec{v}_m) = \nabla \cdot \overline{\overline{S}}_m + \varepsilon_m \rho_m \vec{g} + \vec{I}_{0m} - \sum_{\substack{l=1 \\ l \neq m}}^{M} \vec{I}_{ml} \tag{7}$$

where the stress tensor for the mth solid phase is defined by combining the theories of viscous and plastic flow regimes as (Syamlal et al., 1993):

$$\overline{\overline{S}}_m = \begin{cases} -P_m^{\mathrm{p}}\overline{\overline{I}} + \overline{\overline{\tau}}_m^{\mathrm{p}} & \text{if } \varepsilon_0 \leqslant \varepsilon_0^* \\ -P_m^{\mathrm{v}}\overline{\overline{I}} + \overline{\overline{\tau}}_m^{\mathrm{v}} & \text{if } \varepsilon_0 > \varepsilon_0^* \end{cases} \tag{8}$$

Here P_m is the pressure and $\overline{\overline{\tau}}_m$ is the viscous stress in the mth solids phase. The superscript p stands for plastic regime and v for viscous regime. In fluidized-bed simulations, ε_0^* is set to the void fraction at the minimum fluidization. The plastic stresses are calculated using Schaeffer's (1987) formulation:

$$\overline{\overline{\tau}}_m^{\mathrm{p}} = 2\mu_m^{\mathrm{p}}\overline{\overline{D}}_m \tag{9}$$

where

$$\mu_m^{\mathrm{p}} = \frac{P^* \sin\phi}{2\sqrt{I_{2D}}} \tag{10}$$

Here $\overline{\overline{D_m}}$ is the strain rate tensor for the mth phase, I_{2D} is the second invariant of the deviator of the strain rate tensor (see Syamlal et al., 1993), and ϕ is an angle of internal friction. Similar to the functions typically used in plastic flow theories (Jenike, 1987), an arbitrary function that allows a certain amount of compressibility in the solids phase represents the solids pressure term for plastic flow regime (Pritchett et al., 1978):

$$P_m^{\mathrm{p}} = \varepsilon_m P^* \tag{11}$$

where P^* is represented by an empirical power law (Jenike, 1987)

$$P^* = 10^{25}(\varepsilon_0^* - \varepsilon_0)^{10}. \tag{12}$$

In gas–solids flow calculations, solids pressure functions are used to prevent solids from reaching unphysically large solids' volume fractions, greater than the maximum solids packing limit. Gidaspow (1994) discussed that this term becomes of numerical significance only when the void fraction goes below the minimum fluidization void fraction. It also helps to make the system numerically stable because it converts the imaginary characteristics into real values. Physically,

the solids pressure needs to be represented as a step function of solids volume fraction to model the granular media as an incompressible fluid.

In addition, Lun et al. (1984) theory was extended to describe stresses in multiple granular phases in viscous regime. The granular pressure is given by (Syamlal et al., 1993)

$$P_m^{\mathrm{v}} = K_{1m}\ \varepsilon_m^2\ \Theta_m \tag{13}$$

where K_{1m} is a constant, Θ_m is the granular temperature. Additional details about the model formulation are given by Syamlal et al. (1993), and the solution algorithm is described by Syamlal (1998).

2.1. Particle–particle drag with 'hindrance effect'

The particle–particle interaction force $\vec{I}_{lm}$ is written as:

$$\text{For the drag} \quad \vec{I}_{lm} = F_{lm}(\vec{v}_m - \vec{v}_l) \tag{14}$$

$$F_{ml} = \frac{3(1+e_{lm})(\pi/2 + C_{\mathrm{f}lm}\pi^2/8)\varepsilon_l\rho_l\varepsilon_m\rho_m(d_{\mathrm{p}l}+d_{\mathrm{p}m})^2 g_{0_{lm}}|\vec{v}_l - \vec{v}_m|}{2\pi(\rho_l d_{\mathrm{p}l}^3 + \rho_m d_{\mathrm{p}m}^3)} + C_1 P^* \tag{15}$$

In the first term of the coefficient F_{ml}, derived by Syamlal (1987), e_{lm} and $C_{\mathrm{f}lm}$ are the coefficient of restitution and coefficient of friction, respectively, between the lth and mth granular-phase particles. The radial distribution function at contact, $g_{0_{lm}}$, is that derived by Lebowitz (1964) for a mixture of hard spheres:

$$g_{0_{lm}} = \frac{1}{\varepsilon_0} + \frac{3d_{\mathrm{p}l}d_{\mathrm{p}m}}{\varepsilon_0^2(d_{\mathrm{p}l}+d_{\mathrm{p}m})}\sum_{\lambda=1}^{M}\frac{\varepsilon_\lambda}{d_{\mathrm{p}\lambda}} \tag{16}$$

The first term on the right side of Eq. (15) accounts for the momentum transfer between the phases because of collisions and sliding.

During this study it was found that a new term (the second term on the right side of Eq. (15)) is required to account for a "hindrance effect" in dense particulate flow. In the present formulation, a granular medium consisting of two types of particles is described as two distinct phases. When the particles are closely packed and the diameter ratio is such that the fines cannot percolate through the interstices of the packed bed, the description as two separate particulate phases is inadequate. For example, the model would predict that the two types of particles of different densities would segregate even in a packed bed, whereas, in reality, they do not. The particles do not experience any buoyant force from solids pressure gradient and behave as a single phase. One way to model such a system is to treat it as a single phase as though a "phase change" (multiphase to single phase) has occurred. The implementation of such a model is difficult, and the model is expected to be computationally expensive. So we propose the simple expedient of making the particle–particle drag sufficiently large to account for the "hindrance effect" so that the two-phases will move together and, in effect, behave as a single phase.

The "hindrance effect" is a manifestation of the enduring contacts between the particles and cannot be derived using kinetic theory as in the case of the first term in Eq. (15). So we have taken an heuristic approach guided by the frictional flow theory. We expect the rate of increase in the particle–particle drag to be analogous to the stresses in the frictional regime (Eqs. (9) and (10)),

and, hence, proportional to the granular pressure P^* (Eq. (12))—the greater the granular pressure the greater the tendency for the two phases to move together as a single phase. We expect this functional form to allow the prediction of the fluidization behavior of a binary particle system under three conditions:

1. For fluidization velocity $U < u_{mf}$ (minimum fluidization velocity) of small particles, the two initially well-mixed phases should not separate.
2. For u_{mf} of small particles $< U < u_{mf}$ of large particles, the two initially well-mixed phases should separate.
3. For $U > u_{mf}$ of large particles, the two initially well-mixed phases should remain well mixed.

The experimental rate of separation was used to adjust C_1. A value of 0.3 was found to provide the correct initial slope in Fig. 2. With this value our model was able to match all the above three conditions, which partially (i.e., with respect to the change in fluidization velocity) validates the functional form of the "hindrance effect" term. Ideally, a universal value of C_1 is sought, however due to the limited number of simulations done so far by us, this cannot be confirmed.

2.2. Effect of maximum packing voidage

Mixing particles with different sizes leads to an increase in the maximum packing voidage of the bed. For example, if large spherical beads are mixed with smaller spherical beads, the maximum particle volume fraction of the mixture will be greater than the maximum particle volume fraction of either particle type. Fedors and Landel (1979) proposed the following correlations for the maximum packing voidage for a binary mixture of two particle diameters ($d_1 > d_2$) as a function of mixture composition $X_1 = \varepsilon_1/(\varepsilon_1 + \varepsilon_2)$:

if

$$X_1 \leqslant \frac{\varepsilon_1^{\max}}{(\varepsilon_1^{\max} + (1-\varepsilon_1^{\max})\varepsilon_2^{\max})}$$

$$\varepsilon_0^* = 1.0 - \left(\varepsilon_1^{\max} - \varepsilon_2^{\max} + \left[1 - \sqrt{\frac{d_2}{d_1}}\right](1-\varepsilon_1^{\max})\varepsilon_2^{\max}\right)\left(\varepsilon_1^{\max} + (1-\varepsilon_2^{\max})\varepsilon_1^{\max}\right)\frac{X_1}{\varepsilon_1^{\max}} + \varepsilon_2^{\max}$$

otherwise

$$\varepsilon_0^* = 1.0 - \left[1 - \sqrt{\frac{d_2}{d_1}}\right]\left(\varepsilon_1^{\max} + (1-\varepsilon_1^{\max})\varepsilon_2^{\max}\right)(1-X_1) + \varepsilon_1^{\max} \tag{17}$$

These correlations are used for the maximum packing voidage as a function of mixture composition in the granular pressure and particle–particle drag terms in Eqs. (8), (12) and (15).

3. Binary particle simulations in dense regime

The hydrodynamic model equations are solved for a dense bed of binary-dispersed spherical glass beads of 1.5 and 2.5 mm diameter with density of 2524 kg/m^3, as shown in Fig. 1. A solids

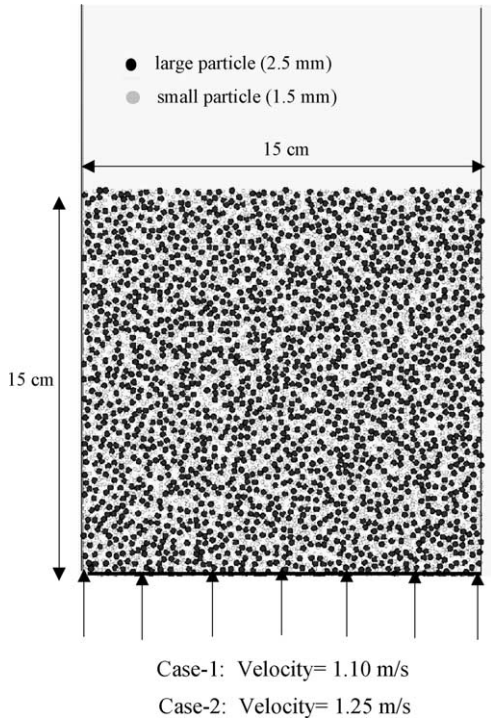

Fig. 1. Schematic of a fluidized bed segregator.

volume fraction of 30% for each of the two granular phases is the initial condition in the bed. The properties of the glass beads (see Table 1) are taken from Goldschmidt et al. (2001). The minimum fluidization velocity (u_{mf}) of the small particles is 0.78 ± 0.02 m/s; that of the large particles is 1.25 ± 0.01 m/s. Two fluidization velocities are used in the simulations: 1.1 m/s, a condition for which segregation should occur; and 1.25 m/s, a condition for which vigorous mixing should occur. These velocities are chosen to demonstrate (a) the segregation of particles when the fluidizing velocity is in between the u_{mf} of two particle types, and (b) vigorous mixing when the fluidizing velocity is equal to or greater than the u_{mf} of the larger particles. The computational grid in the present simulations consists of 15×50 rectangular cells. The convection terms are discretized using the second order accurate superbee method (Leonard and Mokhtari, 1990, Syamlal, 1998).

Table 1
Properties of glass beads used in the simulations

	Small particles	Large particles
Diameter (d_{p1}, d_{p2})	1.5 mm	2.5 mm
Density (ρ_1, ρ_2)	2524 kg/m^3	2524 kg/m^3
Minimum fluidization velocity (u_{mf})	0.78 m/s	1.25 m/s
Coefficient of normal restitution (e)	0.97	0.97
Coefficient of friction (C_{flm})	0.15	0.15

The segregation rate has been quantified by Goldschmidt et al. (2001) using a digital image analysis technique. We used the same procedure as proposed by Goldschmidt et al. (2001) for calculating the average height of the solids phases in the bed:

$$\langle h_m \rangle = \frac{\sum_{\text{cell}} \varepsilon_{m,\text{cell}} h_{\text{cell}}}{\sum_{\text{cell}} \varepsilon_{m,\text{cell}}} \tag{18}$$

where $\varepsilon_{m,\text{cell}}$ is the volume fraction of solids phase m in the cell and h_{cell} is the height of the cell center above the distributor plate; the sum is over all cells in the computational domain. The average height of the two phases predicted by the current model is compared with the experimental data of Goldschmidt et al. (2001) at 1.10 m/s in Fig. 2(a). The rate of segregation is same as the slope of $\langle h \rangle$ vs. time curve in Fig. 2(a). The slope of the curve for large particles was matched up to 18 s, and after which slope became constant. Therefore, the constant C_1 was adjusted to match the initial rate of segregation of the large particles. As described earlier, C_1 is a coefficient in a particle-to-particle interaction force term (I_{lm}: Eqs. (14) and (15)). Hence, this coefficient can be used to match either the slope of large particles or small particles. As a matter of convenience, the slope of large particles was matched in this work. However, C_1 is not expected to change

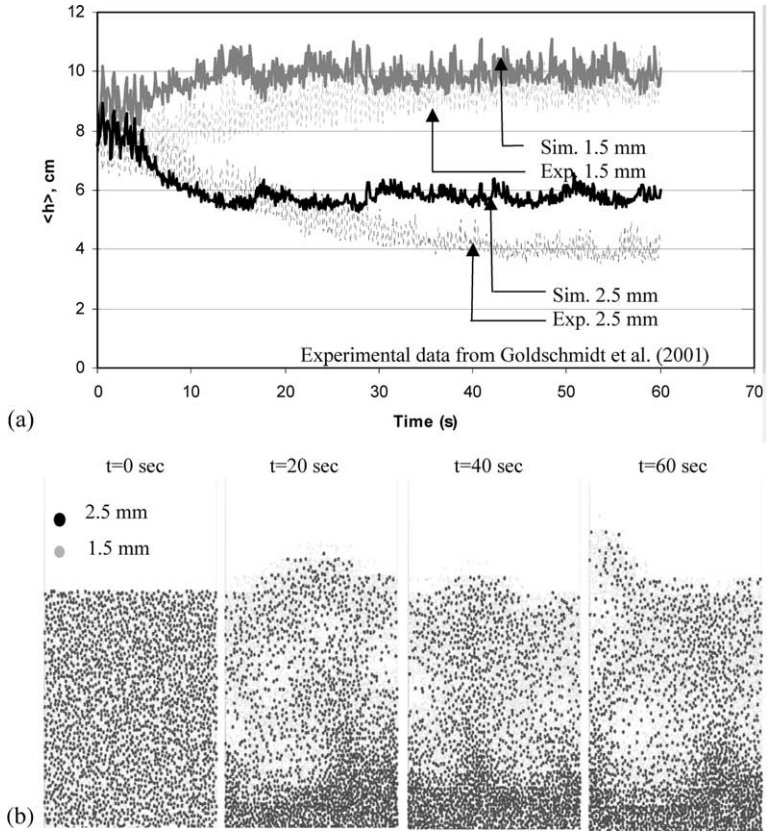

Fig. 2. (a) Comparison of average particle heights obtained from the digital analysis data and the CFD at fluidization velocity at 1.10 m/s and (b) particle segregation predicted by CFD.

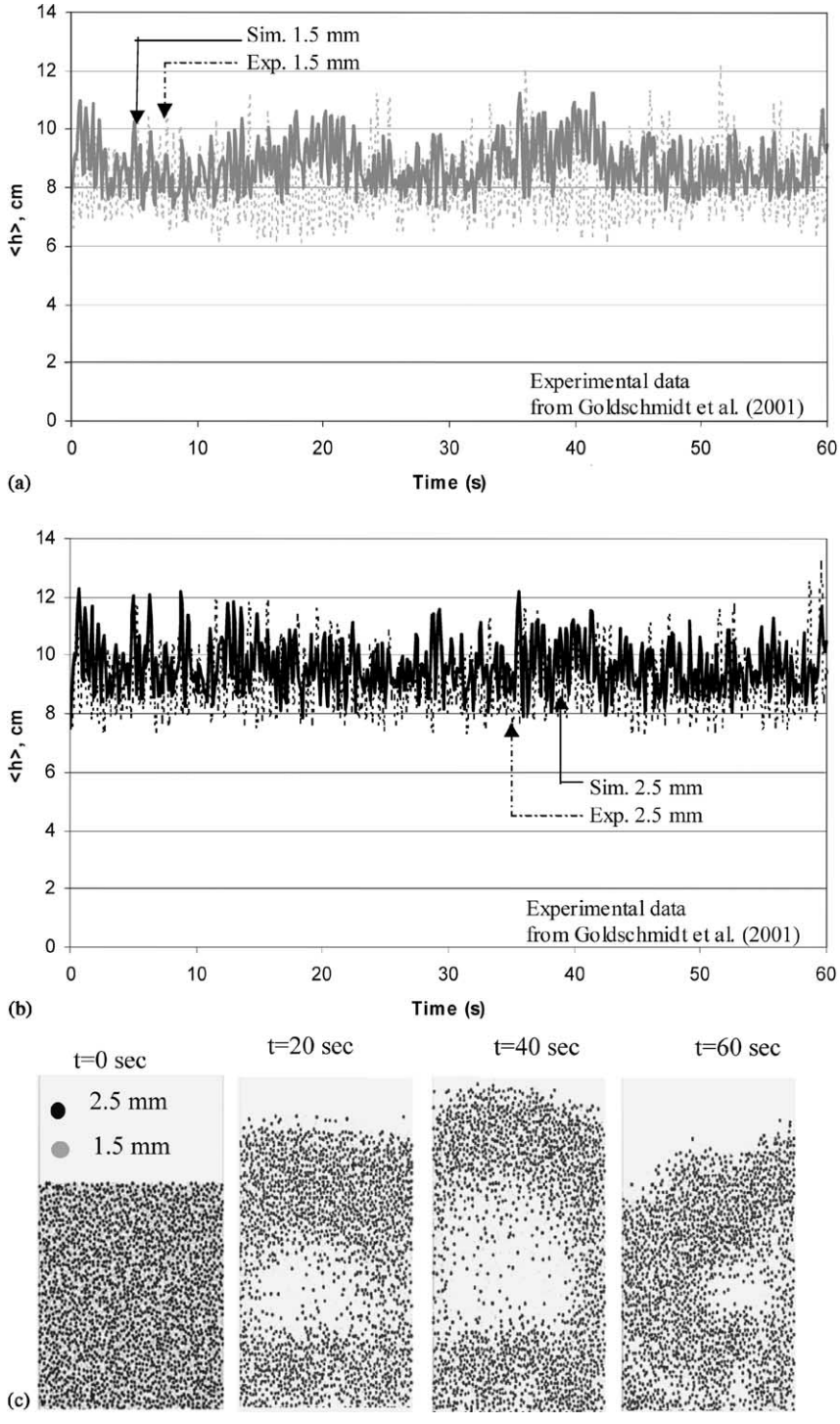

Fig. 3. Comparison of average particle heights obtained from the digital analysis data and the CFD at fluidization velocity at 1.25 m/s for (a) 1.5 mm particles, and (b) 2.5 mm particles. (c) Particle segregation predicted by CFD.

significantly even if the slope of small particles were to be matched. The model captures the slow segregation during the first 8 s followed by a rapid segregation during the next 10 s. At the end of 18 s, the segregation is nearly complete. We continued the simulation up to 60 s to determine the steady state heights of the particulate phases. The height of the small particle layer is well captured by the model. The predicted height of the large particle layer is larger than the experimental value. Eq. (18), used for calculating the heights, does not impose any constraint on the sum of the heights. Thus, a good match in the height of the small particle layer does not imply a good match in the height of the large particle as well.

To aid the visualization of the binary particle system, the number of particles in a grid cell is calculated from the solid volume fraction and a corresponding number of dots are placed randomly in each cell in Fig. 2b. Initially the particles are well mixed. By 20 s a distinct large particle layer forms at the bottom of the bed. That layer appears to be free of small particles. However, the upper layer, which predominantly consists of small particles, contains a fair number of large particles. This causes the over prediction of the height of the large particle layer (Fig. 2a).

The average height of solids phases predicted by the current model at 1.25 m/s is compared with the experimentally measured values in Fig. 3(a) and (b). The corresponding particle number concentration is plotted in Fig. 3(c). The current model predicts the mixing phenomenon very well, unlike previously reported models (e.g., Goldschmidt et al., 2001). The value of the constant C_1 was kept unchanged in this simulation. It can be seen that for 1.25 m/s, the bed starts to bubble and hence leads to the mixing of the particles.

4. Conclusions

A two fluid model is extended to a multi-fluid model. In this model, a primary air phase and two additional particulate phases (each representing a separate class of particle diameters) were tracked in dense regime. A particle-to-particle drag term was developed to account for a ''hindrance'' effect caused by enduring contacts between particles. With this term, the simulations predict no segregation at low fluidization velocities, segregation at intermediate velocities, and vigorous mixing at large fluidizing velocities. The predicted segregation rate for a three-phase fluidized bed matches very well with the measured values.

Acknowledgements

The authors would like to thank Dr. M.J.V. Goldschmidt of Akzo Nobel Chemicals Research in The Netherlands for providing the experimental data in electronic format for the dense bed segregator. His help is gratefully acknowledged.

References

Anderson, T.B., Jackson, R., 1967. A fluid mechanical description of fluidized beds. I&EC Fundam. 6, 527–534.

Chen, A., Grace, J.R., Epstein, N., Lim, C.J., 2002. Steady state dispersion of mono-size, binary and multi-size particles in a liquid fluidized bed classifier. Chem. Eng. Sci. 57, 991–1002.

Fedors, R.F., Landel, R.F., 1979. An empirical method of estimating the void fraction in mixtures of uniform particles of different size. Powder Technol. 23, 225–231.

Gera, D., Gautam, M., Tsuji, Y., Kawaguchi, T., Tanaka, T., 1998. Computer simulation of bubbles in large-particle fluidized beds. Powder Technol. 98, 38–47.

Gidaspow, D., 1994. Multiphase Flow and Fluidization, Continuum and Kinetic Theory Description. Academic Press.

Goldschmidt, M.J.V., Kuipers, J.A.M., van Swaiij, W.P.M., 2001. Segregation in dense gas-fluidised beds: validation of multi-fluid continuum model with non-intrusive digital image analysis measurements. In: 10th Engineering Foundation Conference on Fluidization, Beijing, China, May 20–25, pp. 795–802.

Jenike, A.W., 1987. A theory of flow of particulate solids in converging and diverging channels based on a conical yield function. Powder Technol. 50, 229–236.

Lebowitz, J.L., 1964. Exact solution of generalized Percus–Yevick equation for a mixture of hard spheres. Phys. Rev. A 133, 895–899.

Leonard, B.P., Mokhtari, S., 1990. Beyond first-order upwinding: the ultra sharp alternative for non-oscillatory steady-state simulation of convection. Int. J. Numer. Meth. Eng. 30, 729.

Lun, C.K.K., Savage, S.B., Jeffrey, D.J., Chepurniy, N., 1984. Kinetic theories for granular flow: inelastic particles in couette flow and slightly inelastic particles in a general flow field. J. Fluid Mech. 140, 223–256.

Pritchett, J.W., Blake, T.R., Garg, S.K., 1978. A numerical model of gas fluidized beds. AIChE Symp. Series No. 176, 74, pp. 134–148.

Schaeffer, D.G., 1987. Instability in the evolution equations describing incompressible granular flow. J. Diff. Eq. 66, 19–50.

Syamlal, M., 1998. MFIX Documentation: Numerical Techniques. DOE/MC-31346-5824. NTIS/DE98002029.

Syamlal, M., Rogers, W.A., O'Brien, T.J., 1993. MFIX Documentation and Theory Guide, DOE/METC94/1004, NTIS DE94000087. Electronically available from: http://www.mfix.org.

Syamlal, M., 1987. The particle–particle drag term in a multiparticle model of fluidization. DOE/MC/21353-2373, NTIS/DE87006500.

Tsuji, Y., Kawaguchi, T., Tanaka, T., 1993. Discrete particle simulation of two-dimensional fluidized bed. Powder Technol. 77, 79–87.